Supplementary information to "Development of resistance to type II JAK2 inhibition in MPN depends on AXL kinase and is targetable"

Tamara Codilupi[1]*, Jakub Szybinski[1]*, Stefanie Arunasalam*[1,2,3], Sarah Jungius[1,2,3], Andrew C. Dunbar[4], Simona Stivala[1], Sime Brkic[1], Camille Albrecht[1,2,3], Lenka Vokalova[1,2,3], Julie L. Yang[4], Katarzyna Buczak[5], Nilabh Ghosh[1], Jakob R. Passweg[6], Alicia Rovo[3], Anne Angelillo-Scherrer[3], Dmitry Pankov[7], Stefan Dirnhofer[8], Ross L. Levine[4], Richard Koche[4], Sara C. Meyer[1,2,3,**]

[1]Department of Biomedicine, University Hospital Basel and University of Basel, Basel, Switzerland; [2]Department for Biomedical Research, University of Bern, Bern, Switzerland; [3]Department of Hematology and Central Hematology Laboratory, Inselspital, Bern University Hospital, University of Bern, Bern, Switzerland; [4]Human Oncology and Pathogenesis Program and Leukemia service, Memorial Sloan Kettering Cancer Center, New York, NY, USA; [5]Proteomics Core Facility Biozentrum, University of Basel, Basel, Switzerland; [6]Division of Hematology, University Hospital Basel, Basel, Switzerland; [7]Immunology Program, Sloan-Kettering Institute, Memorial Sloan-Kettering Cancer Center, New York, NY; [8]Department of Pathology, University Hospital Basel, Basel, Switzerland; *These authors contributed equally. **Corresponding author.

Supplementary tables

Supplementary table S1: shRNA sequences

shRNA Name	Target sequence
shAXL-1	CGAAATCCTCTATGTCAACAT
shAXL-2	AGAACAGCGAGATTTATGACTA

Supplementary table S2: Oligos for RT-qPCR

Oligo Name	Sequence
DUSP6 FW	ACCGACACAGTGGTGCTCTA
DUSP6 REV	AACTTACTGAAGCCACCTTCCA
ETV5 FW	CTGCGTCGATTCAGAAGTGC
ETV5 REV	CCAGTCTCTCAGGCACAACA
AXL FW	AGAACATTAGTGCTACGCGG
AXL REV	GCCTTAGCCCTATGTCCATTAG
GAPDH FW	GACAGTCAGCCGCATCTTCT
GAPDH REV	GCCCAATACGACCAAATCCGT

Supplemental table S3: RRID of resources

Resource	RRID	Source
Antibodies		
pJAK2	2617123	Cell Signaling 3776
JAK2	2128522	Cell Signaling 3230
pERK1/2	2315112	Cell Signaling 4370
ERK1/2	390779	Cell Signaling 4695
pMEK1/2	2138017	Cell Signaling 9154
MEK1/2	331778	Cell Signaling 9126
pSTAT3	2491009	Cell Signaling 9145
STAT3	331757	Cell Signaling 9139
pSTAT5	823649	Cell Signaling 9359
STAT5	2737403	Cell Signaling 94205
pAXL	10544794	Cell Signaling 5724
AXL	11217435	Cell Signaling 8661
actin	2242334	Cell Signaling 3700
Plasmid		
pLKO-Tet-On	Addgene_21915	Addgene plasmid # 21915
Cell lines		
SET2	CVCL_2187	Originally as generous gift from R. L. Levine
UKE1	CVCL_0104	Originally as generous gift from R. L. Levine
Ba/F3 Jak2V617F EPOR	CVCL_0161	Originally as generous gift from R. L. Levine
Software and algorithms		
SynergyFinder	SCR_019318	
Flowjo	SCR_008520	
Progenesis QI	SCR_018923	
Limma	SCR_010943	
Sequence Read Archive	SCR_001370	
GraphPad	SCR_002798	

Supplementary methods

Phosphoproteomics raw data processing. Acquired raw-files were imported into the Progenesis QI software (v2.0, Nonlinear Dynamics Limited), which was used to extract peptide precursor ion intensities across all samples applying the default parameters. The generated mgf-file was searched using MASCOT against a human database (consisting of 40700 forward and reverse protein sequences downloaded from Uniprot on 20200417) and 392 commonly observed contaminants using the following search criteria: full tryptic specificity was required (cleavage after lysine or arginine residues, unless followed by proline); 3 missed cleavages were allowed; carbamidomethylation (C) was set as fixed modification; oxidation (M) and phosphorylation (STY) were applied as variable modifications; mass tolerance of 10 ppm (precursor) and 0.02 Da (fragments). The database search results were filtered using the ion score to set the false discovery rate (FDR) to 1% on the peptide and protein level, respectively, based on the number of reverse protein sequence hits in the datasets. Quantitative analysis results from label-free quantification were processed using the SafeQuant R package v.2.3.2. to obtain peptide relative abundances (1). This analysis included global data normalization by equalizing the total peak/reporter areas across all LC-MS runs, data imputation using the knn algorithm, summation of peak areas per protein and LC-MS/MS run, followed by calculation of peptide abundance ratios. Only isoform specific peptide ion signals were considered for quantification. To meet additional assumptions (normality and homoscedasticity) underlying the use of linear regression models and t-Tests, MS-intensity signals were transformed from the linear to the log-scale. The summarized peptide expression values were used for statistical testing of between condition differentially abundant peptides. Here, empirical Bayes moderated t-Tests were applied, as implemented in R/Bioconductor limma package (http://bioconductor.org/packages/release/bioc/html/limma.html). The resulting p-values were adjusted for multiple testing using the Benjamini-Hochberg method.

RNA sequencing. Upon sequencing on Illumina NovaSeq 6000 (Illumina), reads were quality-checked with FastQC quality control tool (2) and adapters trimmed using TrimGalore v.0.4.5 (3) (Alignment was performed with Spliced Transcripts Alignment to a Reference tool (4) (STAR, release 2.4.2a) using GENCODE genome assembly (GRCH38.p12). Raw read count tables were created with HTSeq v0.9.1 (5). Differential gene expression was assessed using DESeq2 software (6) and considered significant at q-values <0.05 and log2FC>0.5. Heatmaps were generated with R (7) and gene set enrichment assessed with GSEAPreranked v4.1.0 on all transcripts expressed in at least one condition as described (8).

ATAC-sequencing. For analysis of chromatin accessibility, JAK2 inhibitor sensitive (JAKi-S) and resistant cells (JAKi-r, JAKi-R) were processed as described (9). Briefly, $5x10^4$ cells were resuspended in cold Resuspension Buffer (10mM NaCl, 10mM Tris pH=7.5, 3mM MgCl2)

supplemented with 0.1% NP40, 0.1% Tween-20, 0.01% Digitonin. After incubation on ice, resuspension buffer supplemented with 0.1% Tween-20 was added and nuclei isolated by centrifugation. Nuclear pellets were processed with Nextera DNA Library prep kit FC-121-1030 (Illumina) containing Tn5 transposase in TD buffer supplemented with 0.1% Tween-20 and 0.01% digitonin. After 30 min. incubation at 37°C and 1000 rpm, DNA was purified with MinElute Clean-up kit (Qiagene) and libraries prepared by PCR amplification for 12 cycles with barcoded primers. Libraries were purified with PCR purification kit (Qiagen) and sequenced on NovaSeq 6000 (Illumina) on the same run (50 bp, paired end). Nextera adaptors and low-quality sequences were trimmed with TrimGalore version 0.4.5 (3) (and reads were aligned to the reference genome (GENCODE, version GRCh38.p12) with bowtie2 (v2.3.4.1) (10). Reads were de-duplicated with MarkDuplicates in Picard Tools v.2.16.0 (https://broadinstitute.github.io/picard/) and peaks called by MACS2 software with p-value at 0.001 as described (11). A peak atlas was built by filtering all peaks against blacklisted regions (http://mitra.stanford.edu/kundaje/akundaje/release/blacklists/hg38human/hg38.blacklist.bed.gz) and reads were counted over the peak union using featureCounts v.1.6.1 (http://subread.sourceforge.net). Differential peak analysis was performed using the raw count matrix and default parameters in DESeq2 software (6). Enrichment of transcription factor motifs in ATAC-sequencing peak regions was performed with Hypergeometric Optimization of Motif Enrichment (HOMER) algorithm as described(12).

Supplementary references

1. Ahrné E, Glatter T, Viganò C, Von Schubert C, Nigg EA, Schmidt A. Evaluation and improvement of quantification accuracy in isobaric mass tag-based protein quantification experiments. J Proteome Res. American Chemical Society; 2016;15:2537–47.
2. Andrews S. FastQC: a quality control tool for high throughput sequence data. [Internet]. 2010. Available from: https://www.bioinformatics.babraham.ac.uk/projects/fastqc/
3. Krueger F. TrimGalore: adapter trimming to FastQ files [Internet]. 2012. Available from: https://www.bioinformatics.babraham.ac.uk/projects/trim_galore/
4. Dobin A, Davis CA, Schlesinger F, Drenkow J, Zaleski C, Jha S, et al. STAR: ultrafast universal RNA-seq aligner. Bioinformatics. 2013;29:15–21.
5. Anders S, Pyl PT, Huber W. HTSeq-A Python framework to work with high-throughput sequencing data. Bioinformatics. 2015;31:166–9.
6. Love MI, Huber W, Anders S. Moderated estimation of fold change and dispersion for RNA-seq data with DESeq2. Genome Biol. 2014;15:1–21.
7. Team RC. R: A language and environment for statistical computing. R Foundation for Statistical Computing [Internet]. 2022. Available from: https://www.r-project.org/
8. Subramanian A, Tamayo P, Mootha VK, Mukherjee S, Ebert BL, Gillette MA, et al. Gene set enrichment analysis: a knowledge-based approach for interpreting genome-wide expression profiles. Proc Natl Acad Sci U S A. National Academy of Sciences; 2005;102:15545–50.
9. Corces MR, Trevino AE, Hamilton EG, Greenside PG, Sinnott-Armstrong NA, Vesuna S, et al. An improved ATAC-seq protocol reduces background and enables interrogation of frozen tissues. Nat Methods. Nature Publishing Group; 2017;14:959–62.
10. Langmead B, Salzberg SL. Fast gapped-read alignment with Bowtie 2. Nat Methods. 2012;9:357–9.
11. Zhang Y, Liu T, Meyer CA, Eeckhoute J, Johnson DS, Bernstein BE, et al. Model-based analysis of ChIP-Seq (MACS). Genome Biol. Genome Biol; 2008;9.
12. Heinz S, Benner C, Spann N, Bertolino E, Lin YC, Laslo P, et al. Simple Combinations of Lineage-Determining Transcription Factors Prime cis-Regulatory Elements Required for Macrophage and B Cell Identities. Mol Cell. Mol Cell; 2010;38:576–89.

Supplementary figures

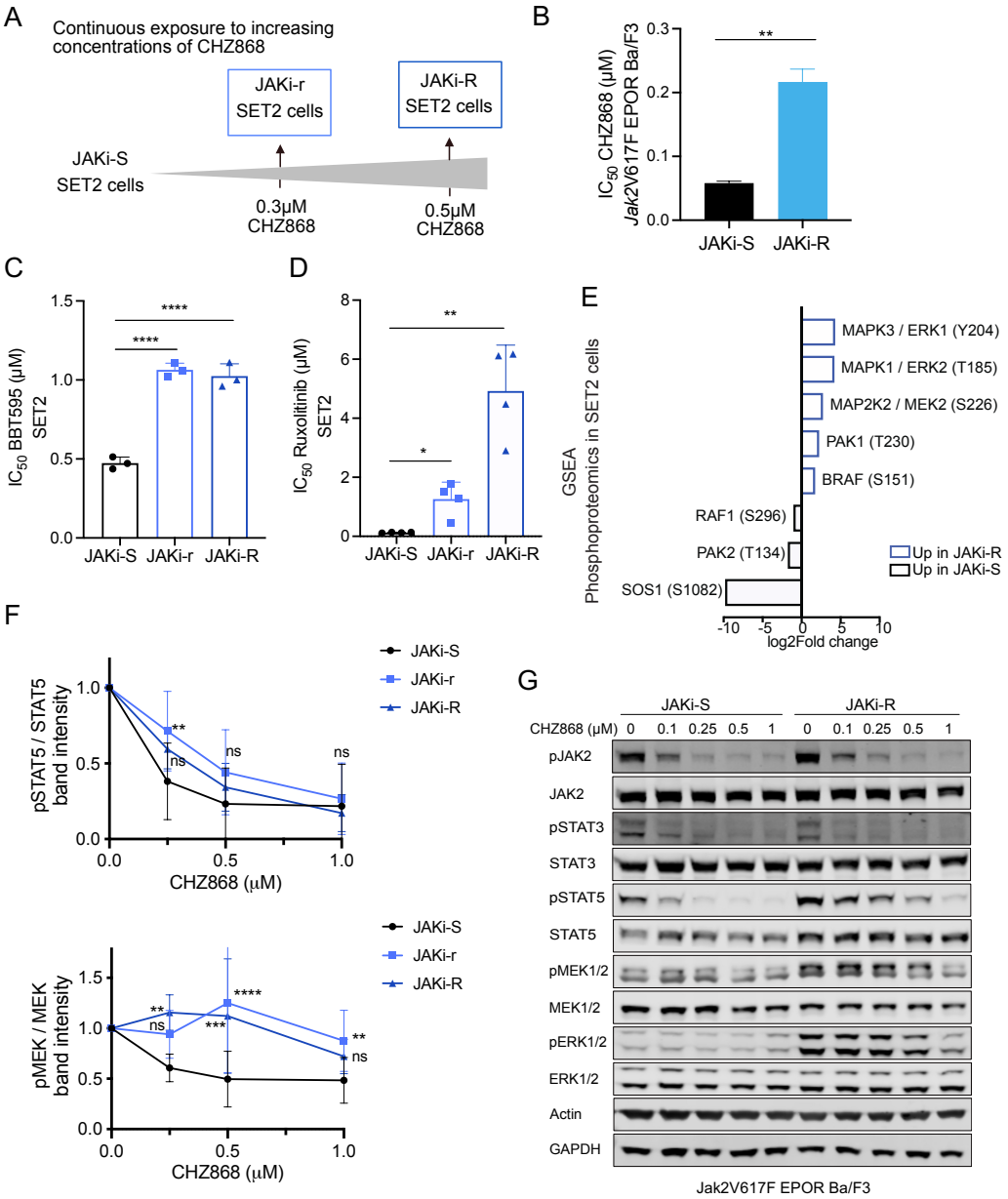

Supplementary figure 1. Characterization of acquired resistance to type II JAK2 inhibition by CHZ868 in MPN cells (supplemental information to Fig. 1). A. JAK2 V617F mutant SET2 cells sensitive to type II JAK2 inhibition with CHZ868 (JAKi-S) were continuously exposed to CHZ868 at increasing concentrations inducing acquired resistance. Two JAK2 inhibitor resistant cell lines were generated and kept at maintenance concentrations of 0.3 μM CHZ868 (JAKi-r) and 0.5 μM CHZ868 (JAKi-R), respectively, for characterization. **B.** In addition, Ba/F3 cells stably expressing Jak2V617F and EPOR sensitive to type II JAK2 inhibition with CHZ868 (JAKi-S) were analogously exposed to CHZ868 and outgrowing resistant cells kept at maintenance concentration of 0.5 μM CHZ868 (JAKi-R). Half-maximal inhibitory concentration (IC_{50}) was significantly increased in JAKi-R Jak2V617F EPOR Ba/F3 cells similarly to the findings in JAK2 inhibitor resistant SET2 cells (n=3). **C.** JAKi-r and JAKi-R SET2 cells also showed resistance to BBT594, a previously developed, less potent type II JAK2 inhibitor, as indicated by increased IC_{50} compared to JAKi-S SET2 (n=3). **D.** JAKi-r and JAKi-R SET2 cells showed resistance to type I JAK2 inhibition with ruxolitinib as indicated by increased IC_{50} compared to JAKi-S SET2 (n=4). **E.** MAPK pathway components including ERK, MEK and BRAF and respective regulators such as SOS showed differential phosphorylation in JAK2 inhibitor resistant as compared to JAK2 inhibitor sensitive cells. Blue: phosphorylation upregulated in JAKi-R cells. Black: phosphorylation upregulated in JAKi-S cells. Specific protein residues are indicated. **F.** Densitometry of phosphoproteins shown by immunoblotting in Figure 1E-F confirmed increased MEK1/2 phosphorylation in JAKi-r and JAKi-R cells exposed to type II JAK2 inhibition with CHZ868 whereas JAKi-S cells showed dose-dependent inhibition of pMEK (lower panel). Densitometry confirmed dose-dependent suppression of JAK2 and STAT5 phosphorylation upon type II JAK2 inhibition with CHZ868 in JAKi-r and JAKi-R cells similarly to JAKi-S cells (upper panel, n=7-9). **G.** Immunoblotting confirmed activated MAPK pathway signaling also in JAK2 inhibitor resistant (JAKi-R) Jak2V617F EPOR Ba/F3 cells in comparison to JAKi-S cells as reflected by pERK1/2 and pMEK1/2 despite exposure to increasing concentrations of type II JAK2 inhibitor CHZ868. JAK2, STAT3 and STAT5 remained inhibited in presence of CHZ868 in JAKi-R Jak2V617F EPOR Ba/F3 cells similarly to JAKi-S cells. Data are presented as mean ± SD and analyzed by one-way ANOVA (C,D,F) or by two-tailed Student t test (B). ns, not significant; *, p ≤0.05; **, p ≤0.01; ***, p ≤0.001; ****, p ≤0.0001.

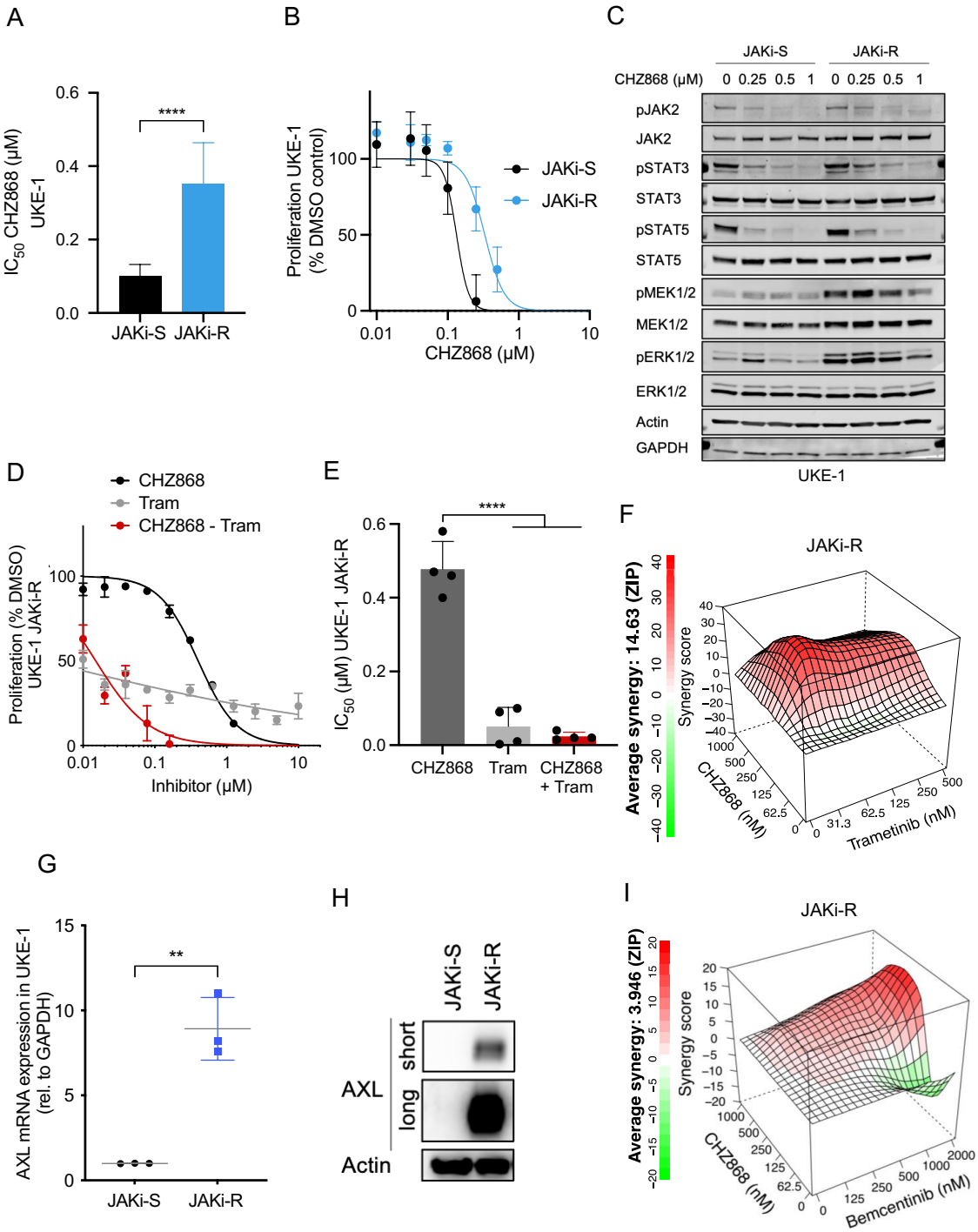

Supplementary figure 2. Acquired resistance to type II JAK2 inhibition in JAK2 V617F UKE-1 cells relates to AXL/MAPK activation. *JAK2* V617F UKE-1 cells developed significantly increased half-maximal inhibitory concentration IC_{50} for type II JAK2 inhibitor CHZ868 upon continuous exposure (JAKi-R) as compared to JAK2 inhibitor sensitive UKE-1 cells (JAKi-S) reflecting acquired resistance (**A**, n=3). Proliferation of JAKi-R UKE-1 cells over 48h was less effectively inhibited by increasing concentrations of CHZ868 as compared to JAKi-S UKE-1 cells (**B**, n=3, representative graph shown). Immunoblotting showed activated MAPK pathway signaling reflected by pERK1/2 and pMEK1/2 in JAKi-R vs. JAKi-S UKE-1 cells upon exposure to increasing concentrations of CHZ868. JAK2, STAT3 and STAT5 remained inhibited in presence of CHZ868 in JAKi-R UKE-1 cells similarly to JAKi-S UKE-1 cells (**C**). Proliferation of JAKi-R UKE-1 cells was inhibited by combined JAK2/MAPK pathway inhibition with CHZ868/trametinib as shown by a representative graph of proliferation capacity upon 48h inhibitor exposure (**D**). IC_{50} was significantly reduced by combined CHZ868/trametinib in JAKi-R UKE-1 cells (**E**, n=4). Zero interaction potential (ZIP) analysis of type II JAK2 inhibition with CHZ868 and MAPK pathway inhibition with trametinib showed positive synergy scores in JAKi-R UKE-1 cells (**F**, mean of n=2 experiments shown for ZIP score along with representative graph). AXL expression was significantly increased in JAKi-R vs. JAKi-S UKE-1 cells relative to GAPDH on mRNA level (**G**, n=3) and on protein level (**H**, long: long exposure time, short: short exposure time). ZIP analysis of CHZ868 with AXL inhibitor bemcentinib in JAKi-R UKE-1 cells showed positive synergy scores (**I**, mean of n=2 experiments shown for ZIP scores along with representative graph). Data are presented as mean ± SD and analyzed by one-way ANOVA (panels D, E) or two-tailed Student t test (A, B, G). ns, not significant; *, p ≤0.05; **, p ≤0.01; ****, p ≤0.0001.

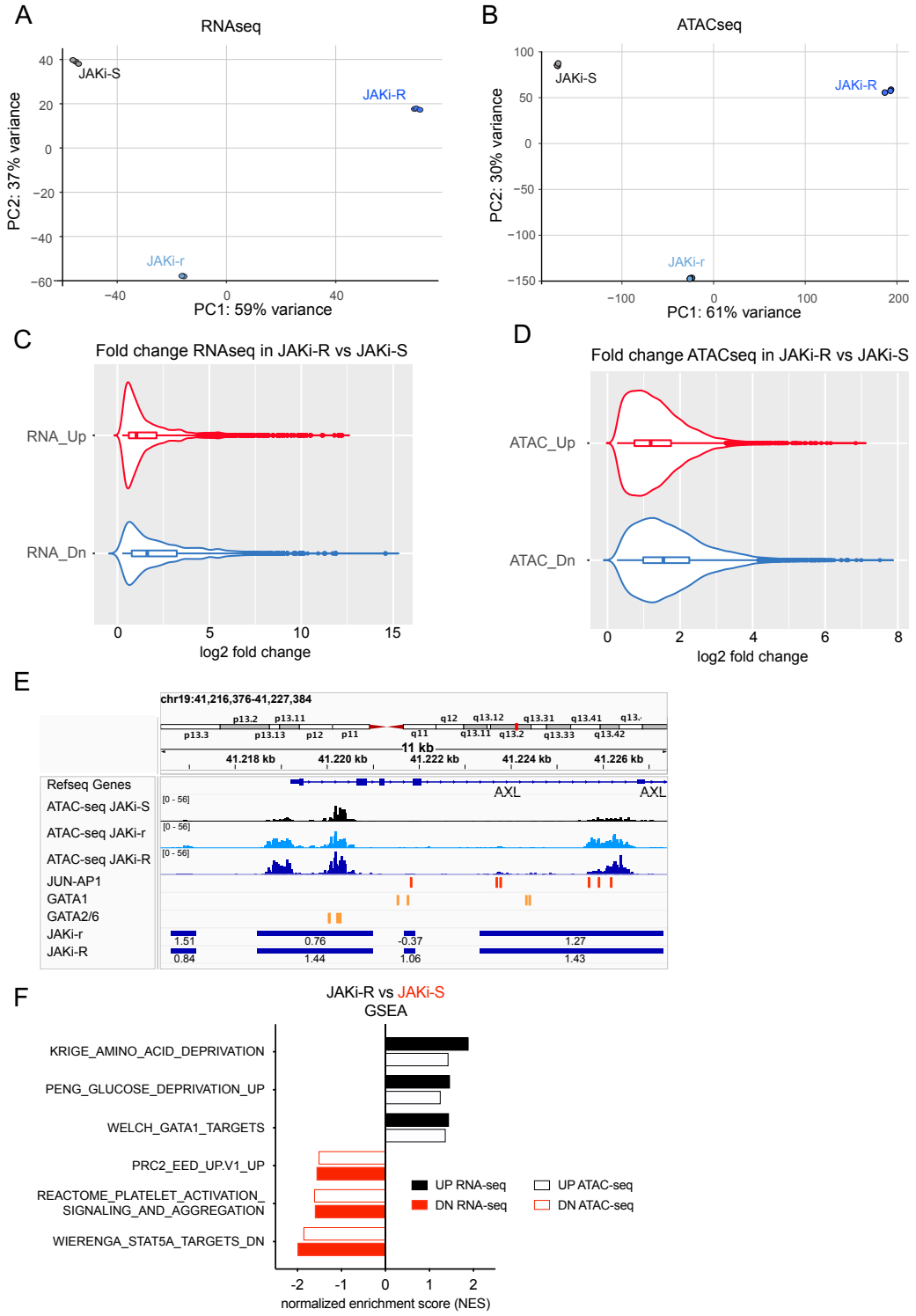

Supplementary Figure 3. Analyses of transcriptional programs and histone occupancy in acquired resistance to type II JAK2 inhibition (supplemental information to Fig. 2). A. Principal Component analysis of JAK2 inhibitor resistant (JAKi-r, JAKi-R) as compared to JAK2 inhibitor sensitive (JAKi-S) SET2 cells based on mRNA expression patterns showed that resistant cells segregated from sensitive cells in PC1 (n=3). **B.** Principal Component analysis of JAK2 inhibitor resistant (JAKi-r, JAKi-R) as compared to JAK2 inhibitor sensitive (JAKi-S) SET2 cells based on histone occupancy patterns assessed by ATAC sequencing showed that resistant cells segregated from sensitive cells in PC1 (n=3). **C.** Violin plots showing absolute log2(FoldChange) of gene expression from RNA sequencing data for upregulated (Up) and downregulated (Dn) genes in JAKi-R as compared to JAKi-S cells. **D.** Violin plots showing absolute log2(FoldChange) of chromatin accessibility from ATAC sequencing data for chromatin regions with increased (Up) or decreased (Dn) accessibility in JAKi-R as compared to JAKi-S cells. Mean, Standard Deviation and Outlier values are indicated within the integrated boxplot. **E.** Analysis of chromatin state (top traces, ATAC-seq) and transcription factor binding motifs (middle traces) at the AXL gene region showed higher chromatin accessibility in the AXL locus overlapping with the presence of JUN-AP1 and GATA bindings motifs in JAKi-R as compared to JAKi-S cells. Numbers indicate the log2(fold change) of JAKi-R as compared to JAKi-S cells. **F.** Differentially accessible chromatin regions between JAKi-R vs. JAKi-S cells were explored with GSEA analysis showing enrichment for GATA transcription factor binding site exposure in JAKi-R cells.

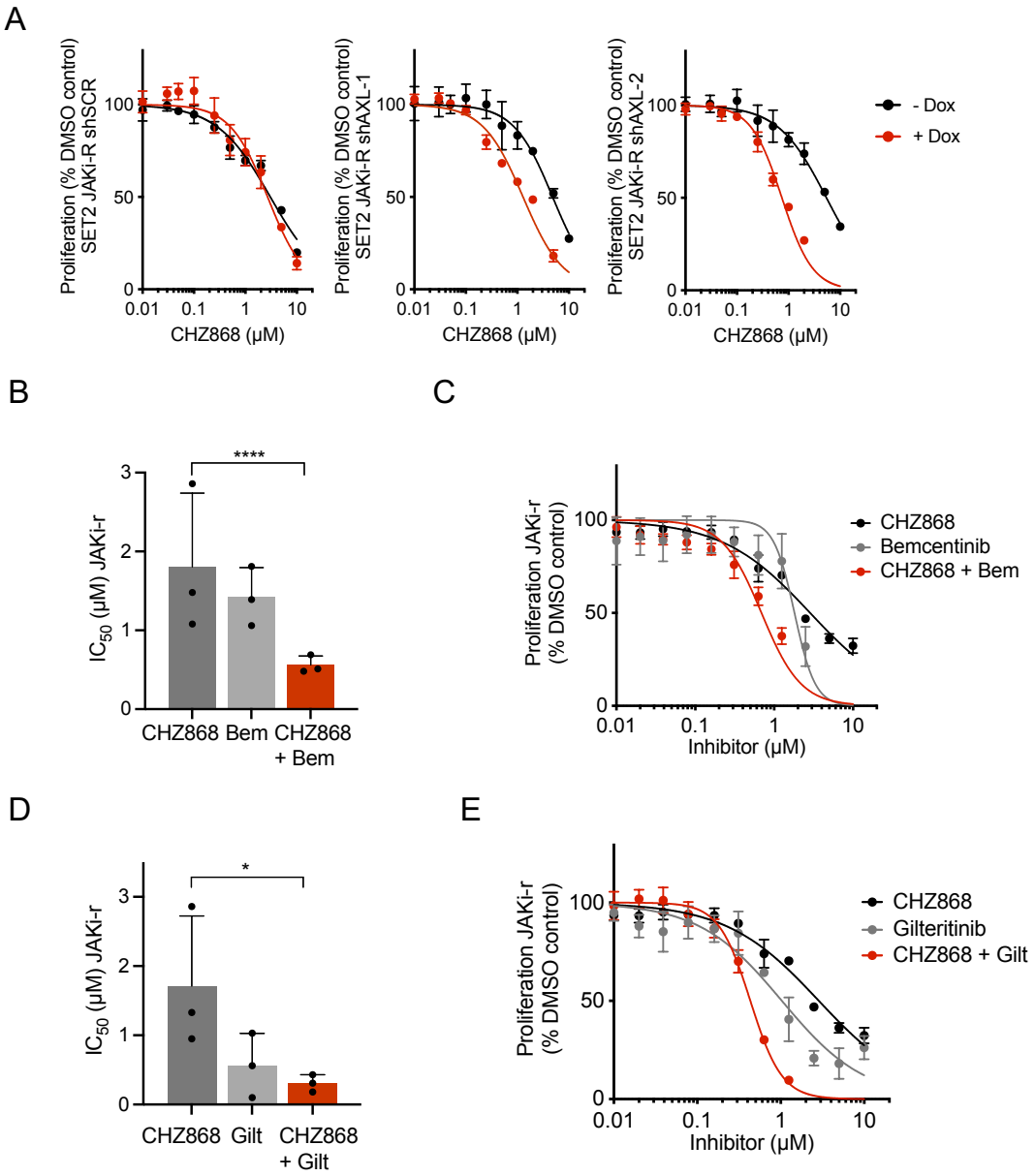

Supplementary figure 4. Acquired resistance to type II JAK2 inhibition is dependent on AXL tyrosine kinase (supplemental information to Fig. 3). A. Representative graph with reduced proliferation of JAKi-R SET2 cells upon shRNA-mediated AXL depletion with shAXL-1 or shAXL-2 (middle and right panel) as compared to shSCR control (left panel) upon doxycycline induction (+dox). Non-induced control (-dox). **B.** Significantly reduced half-maximal inhibitory concentration (IC_{50}) values in JAKi-r SET2 cells were achieved upon combined exposure with the AXL inhibitor bemcentinib and type II JAK2 inhibition with CHZ868 (n=3). **C.** Representative graph showing reduced proliferation of JAKi-r SET2 cells exposed to combined JAK2 / AXL inhibition with CHZ868 / bemcentinib as compared to CHZ868 as a single agent. **D.** Significantly reduced IC_{50} values in JAKi-r SET2 cells were achieved upon combined exposure with the AXL/FLT3 inhibitor gilteritinib and type II JAK2 inhibition with CHZ868 (n=3). **E.** Representative graph showing reduced proliferation of JAKi-r SET2 cells exposed to combined JAK2 / AXL inhibition with CHZ868 / gilteritinib as compared to CHZ868 as a single agent. Data are presented as mean ±SD and analyzed by one-way ANOVA (B, D). ns, not significant; *, p ≤0.05; **, p ≤0.01; ***, p ≤0.001; ****, p ≤0.0001.

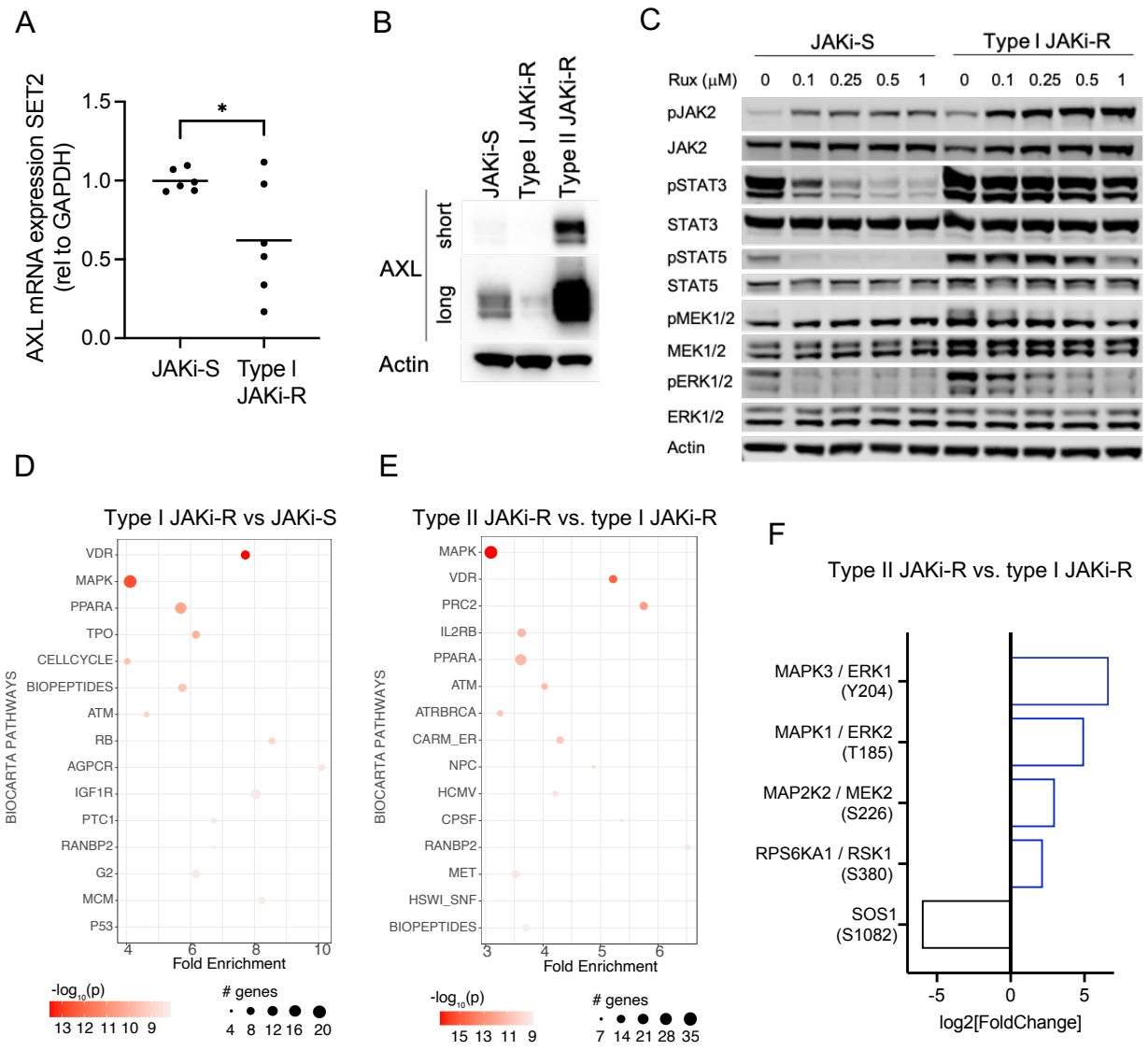

Supplementary figure 5. MAPK activation in type I JAK2 inhibitor resistance does not relate to AXL upregulation. Expression of AXL was assessed in type I JAK2 inhibitor resistant (JAKi-R) as compared to JAK2 inhibitor sensitive (JAKi-S) SET2 cells on RNA (**A**) and protein levels (**B**) and was not increased in resistant vs. sensitive settings. JAK2, STAT3/5 and MAPK signaling was assessed in type I JAKi-R vs JAKi-S cells by immunoblotting upon exposure to increasing concentrations of the type I JAK2 inhibitor ruxolitinib at 0.1-1uM demonstrating reactivation of JAK2, STAT3/STAT5 and MAPK signaling in resistant vs. sensitive settings as previously reported (**C**). Phosphoproteomic mass spectrometry followed by pathway analysis with PathfindR confirmed MAPK pathway activation in type I JAKi-R SET2 cells vs. JAKi-S cells based on Biocarta (**D**). Phosphoproteomic mass spectrometry followed by pathway analysis of type II JAKi-R SET2 cells vs. type I JAKi-R cells showed further enrichment of MAPK pathway alterations in type II JAKi-R cells with positive enrichment of ERK, MEK and RSK and negative enrichment of MAPK regulator SOS (**E-F**). Blue: phosphorylation upregulated in type II JAKi-R cells. Black: phosphorylation upregulated in type I JAKi-R cells. Specific protein residues are indicated in brackets. Data in A were assessed by two-tailed Student t test and p ≤0.05 (*) considered statistically significant.

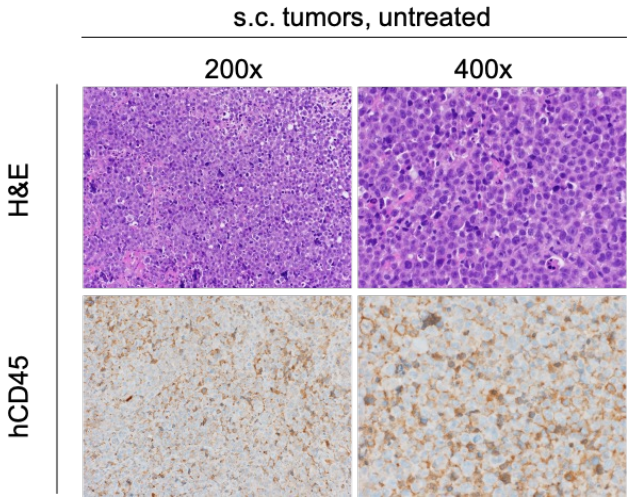

Supplementary figure 6. In vivo model of type II JAK2 inhibitor resistance with subcutaneous engraftment of resistant cells (supplemental information to Fig. 4). Subcutaneous (s.c.) tumors were stained by hematoxylin and eosin (H&E, upper panel) and immunohistochemistry for human CD45 (hCD45, lower panel) confirming tumors composed of JAK2 inhibitor resistant SET2 cells injected s.c. into NSG mice. Representative images at magnification of 200x and 400x are shown.

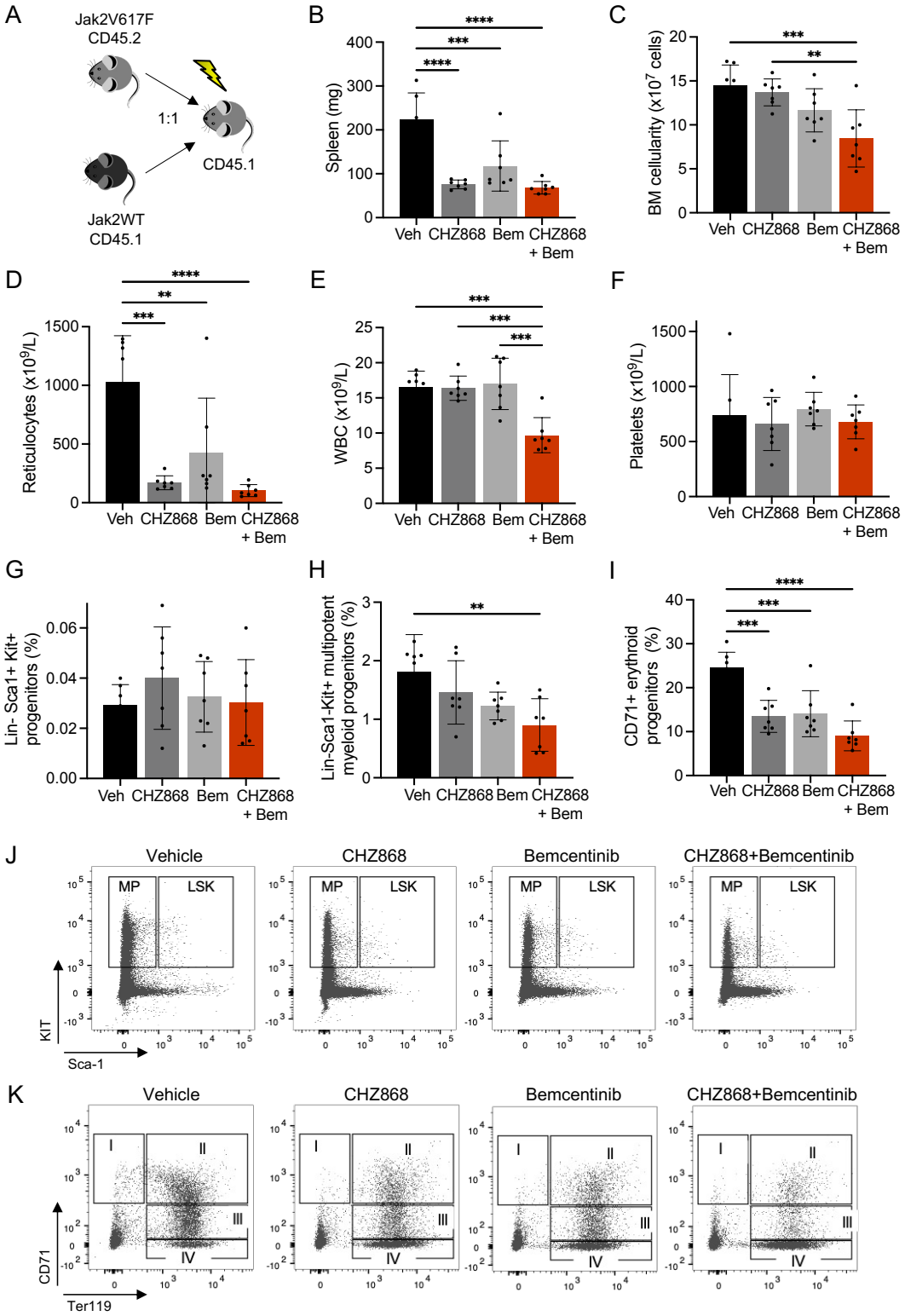

Supplementary figure 7. AXL inhibition enhances efficacy of type II JAK2 inhibition in a *Jak2* V617F MPN mouse model in vivo. *Jak2*V617F CD45.2 and *Jak2* WT CD45.1 bone marrow cells (BM) mixed at 1:1 ratio were transplanted into CD45.1 C57BL/6 recipients. Mice were randomized 10 weeks after transplant according to blood counts and treated for 2 weeks with vehicle, type II JAK2 inhibitor CHZ868 at low dosage of 15mg/kg, AXL inhibitor bemcentinib at 50mg/kg or combined CHZ868/bemcentinib. Spleen weight, BM cellularity, peripheral blood counts and BM hematopoietic progenitors were assessed (**A**). Splenomegaly and BM hypercellularity were moderated by type II JAK2 inhibitor as well as by AXL inhibitor treatment, while combined type II JAK2/AXL inhibition induced most pronounced effects (**B-C**). Reticulocytosis and leukocytosis were corrected by combined type II JAK2 / AXL inhibitor treatment, while platelets remained in the normal range as usually seen in this model at early time-points of 10-12 weeks after transplant (**D-F**). Expanded Lin-Sca1-Kit+ multipotent myeloid and CD71+ erythroid progenitors were reduced by CHZ868 as well as by bemcentinib, which enhanced effects of CHZ868 when applied in combination. Lin-Sca1+Kit+ (LSK) populations were not significantly altered (**G-I**). Representative dot plots are shown **(J-K)**. n=7 per group, data presented as mean ± SD and analyzed by one-way ANOVA. *, p ≤0.05; **, p ≤0.01; ***, p ≤0.001; ****, p ≤0.0001. Roman numerals in (K) indicate erythroid progenitor populations (I: CD71+ Ter119-, II: CD71+Ter119+, III: CD71lowTer119+, IV: CD71-Ter119+).

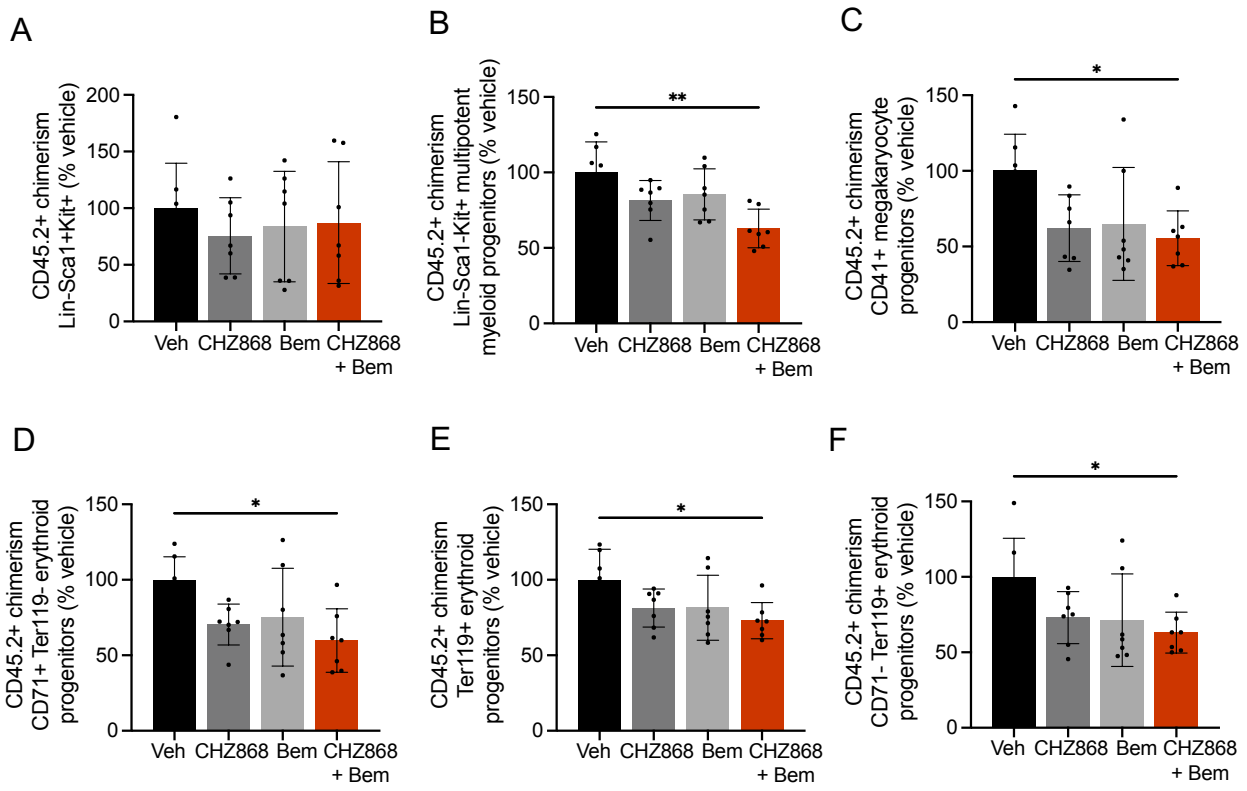

Supplementary figure 8. AXL inhibition promotes reduction of *Jak2*V617F mutant hematopoietic progenitor cell proportions in a *Jak2* V617F MPN mouse model in vivo. *Jak2*V617F CD45.2 and *Jak2* WT CD45.1 bone marrow cells (BM) mixed 1:1 were engrafted into CD45.1 C57BL/6 recipients which were randomized and treated for 2 weeks with vehicle, type II JAK2 inhibitor CHZ868 at low dosage of 15mg/kg, AXL inhibitor bemcentinib at 50mg/kg or combined CHZ868/bemcentinib. While CHZ868 at low dosage of 15 mg/kg and bemcentinib at 50 mg/kg showed only subtly modified CD45.2/CD45 chimerism in Lin-Sca1+Kit+ (LSK) stem/progenitors (**A**), in Lin-Sca1-Kit+ multipotent myeloid (MP) progenitors (**B**) as well as in CD41+ megakaryocytic (**C**) and CD71+ and/or Ter119+ erythroid progenitor cells (**D-F**), AXL inhibition with bemcentinib enhanced type II JAK2 inhibitor effects on Jak2V617F mutant cell proportion as reflected by significant reduction of CD45.2/CD45 chimerism. Data are presented as mean ± SD and analyzed by one-way ANOVA. *, $p \leq 0.05$; **, $p \leq 0.01$.

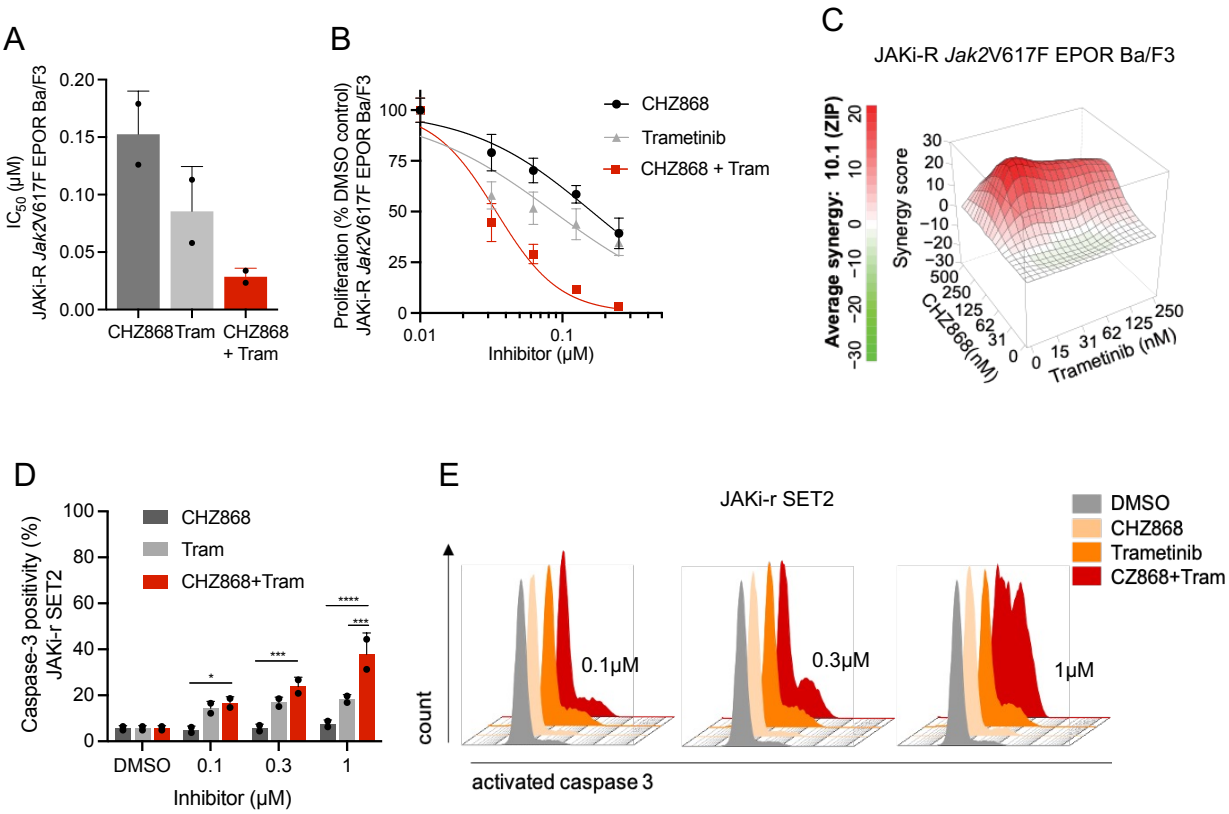

Supplementary figure 9. **MAPK inhibition abrogates acquired resistance to type II JAK2 inhibition in SET2 cells as well as in *Jak2*V617F EPOR Ba/F3 cells (supplemental information to Fig. 5). A.** Half-maximal inhibitory concentration IC_{50} was significantly reduced by combined CHZ868 / trametinib in JAK2 inhibitor resistant (JAKi-R) *Jak2*V617F EPOR Ba/F3 cells (n=2). **B.** Proliferation of JAKi-R *Jak2*V617F EPOR Ba/F3 cells was effectively inhibited by combined JAK2 / MAPK pathway inhibition with CHZ868 / trametinib as shown by a representative graph of proliferation capacity upon 48h exposure of inhibitor exposure. **C.** Synergy analysis of type II JAK2 inhibition with CHZ868 and MAPK pathway inhibition with trametinib showed positive synergy in JAKi-R *Jak2*V617F EPOR Ba/F3 cells. Mean of n=2 experiments is shown for synergy score along with a representative graph. **D.** Apoptotic cell death reflected by positivity for caspase-3 was induced by combined JAK2 / MAPK pathway inhibition by CHZ868 / trametinib in JAKi-r SET2 cells upon 48h exposure to inhibitors (n=2). **E.** Representative histograms of caspase-3 positivity in JAKi-r SET2 cells are shown. Data are presented as mean ± SD and analyzed by one-way ANOVA (A,G,I). ns, not significant; *, p ≤0.05; **, p ≤0.01; ***, p ≤0.001; ****, p ≤0.0001.

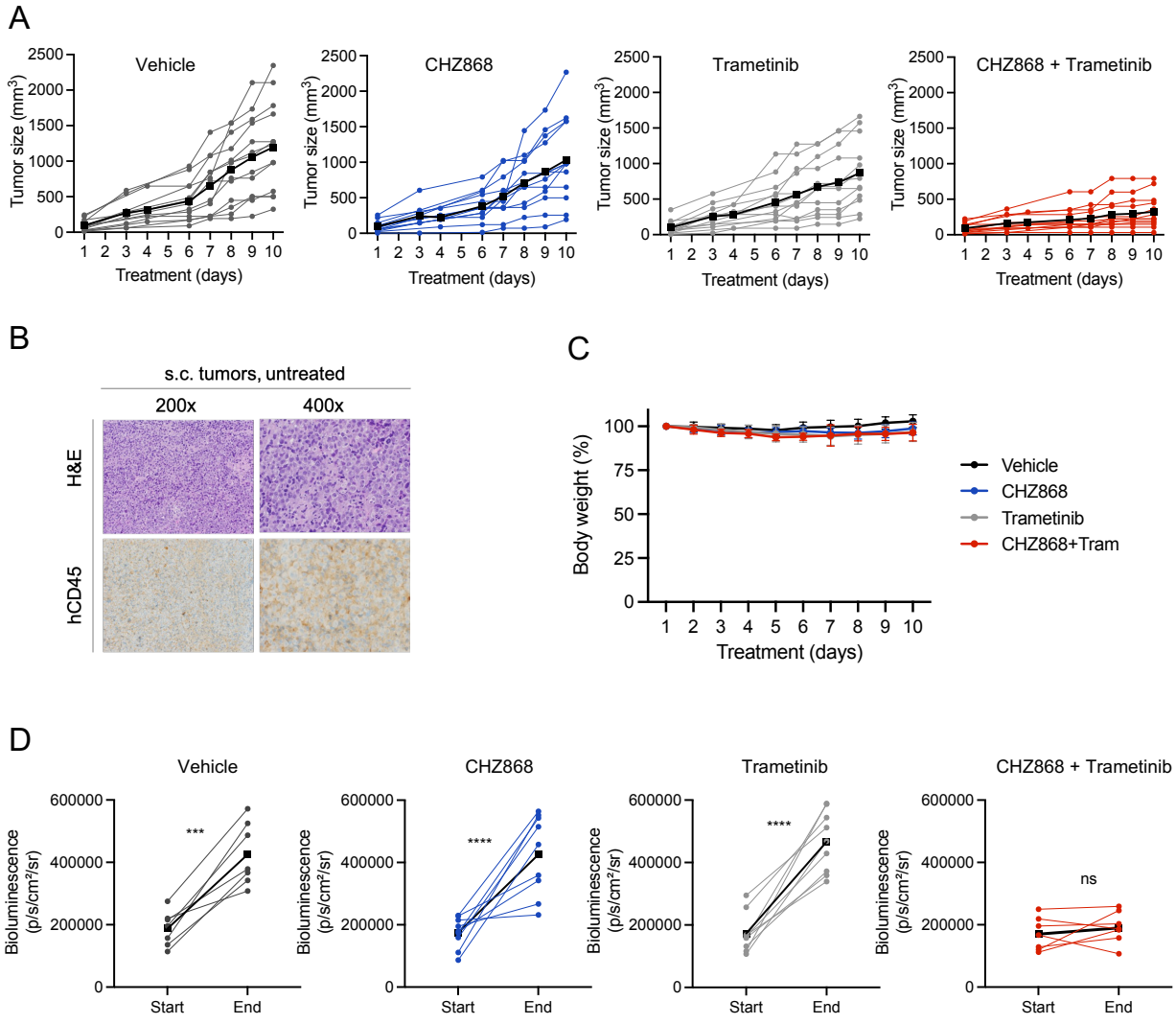

Supplementary figure 10. Targeting MAPK pathway abrogates acquired resistance to type II JAK2 inhibition in vivo upon subcutaneous and intravenous engraftment (supplemental information to Fig. 6). A. Subcutaneous tumor growth in individual mice is shown for each treatment group. Black lines indicate the average tumor size per group. Animals were treated orally with type II JAK2 inhibitor CHZ868 15mg/kg qd, MAPK inhibitor trametinib (tram) 0.3mg/kg qd, combined CHZ868 15mg/kg qd / MAPK inhibitor trametinib 0.3mg/kg qd or vehicle control. Treatment was initiated at 100mm^3 tumor size and continued until maximal tumor size was reached in vehicle treated mice. Combined CHZ868/trametinib almost suppressed tumor growth in the treated mice (n=13/group). **B.** Subcutaneous (s.c.) tumors were stained by hematoxylin and eosin (H&E, upper panel) and immunohistochemistry for human CD45 (hCD45, lower panel) confirming tumors composed of JAK2 inhibitor resistant SET2 cells injected s.c. into NSG mice. Representative images at magnification of 200x and 400x are shown. **C.** Average body weight per treatment group. **D.** Bioluminescent signal in individual mice injected with JAKi-R cells intravenously is shown at initiation (start) and completion (end) of treatment for each treatment group. Black lines indicate the average bioluminescent signal per group. A significant increase of bioluminescent signal over time reflecting JAKi-R cell expansion was observed for all groups except for mice treated with combined JAK2 / MAPK inhibition with CHZ868 15mg/kg qd and trametinib 0.3mg/kg qd. Data are presented as mean ± SD and analyzed by one-way ANOVA (A,G,I). ns, not significant; *, p ≤0.05; **, p ≤0.01; ***, p ≤0.001; ****, p ≤0.0001.

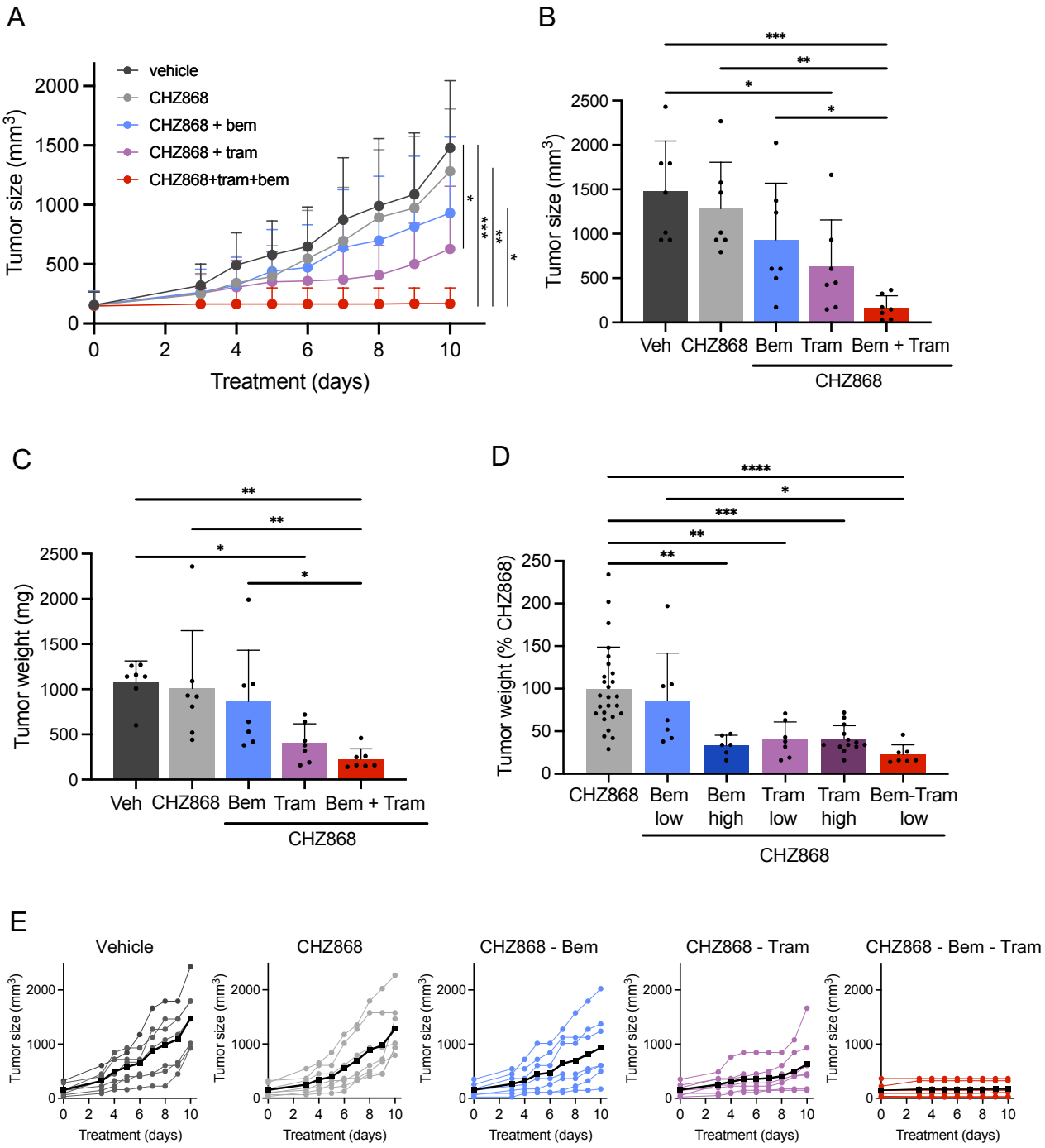

Supplementary figure 11. Combination of AXL and MAPK inhibitors at reduced dose in context of type II JAK2 inhibitor resistance in JAKi-R CDX mouse model in vivo. JAK2 inhibitor resistant SET2 cells (JAKi-R) were injected subcutaneously into the flank of NSG mice. Animals were treated orally with CHZ868 15mg/kg, AXL inhibitor bemcentinib (bem) 35mg/kg bid, MAPK inhibitor trametinib (tram) 0.2mg/kg qd, the indicated combinations or vehicle control (n=7 mice per group). Tumor size over time showed moderate inhibition of tumor growth in mice treated with CHZ868 and reduced dose of bemcentinib or trametinib, while tumor progression was nearly completely inhibited when AXL and MAPK inhibition were combined (**A**). Tumor size and weight at end of treatment showed significant efficacy by combined AXL / MAPK inhibition at reduced dose in the setting of type II JAK2 inhbitor resistance (**B-C**). Tumor weights compared across treatment studies in subcutaneously engrafted NSG mice treated with bemcentinib low (35mg/kg bid), bemcentinib high (50mg/kg bid), trametinib low (0.2mg/kg qd) and trametinib high (0.3mg/kg qd) as compared to CHZ868 (15 mg/kg qd) (**D**). Subcutaneous tumor growth in individual mice is shown for each treatment group. Black lines indicate average tumor size per group (**E**). Data are presented as mean ± SD and analyzed by one-way ANOVA. ns, not significant; *, p ≤0.05; **, p ≤0.01; ***, p ≤0.001; ****, p ≤0.0001.

A

Pt	MPN Subtype	Driver Mutation	Sex	Age (years)	Inhibitor exposure
1	PV	JAK2 V617F	f	74	JAK2/AXL JAK2/MAPK
2	PV	JAK2 V617F	m	39	JAK2/AXL
3	PV	JAK2 V617F	m	40	JAK2/MAPK
4	ET	JAK2 V617F	m	69	JAK2/AXL JAK2/MAPK

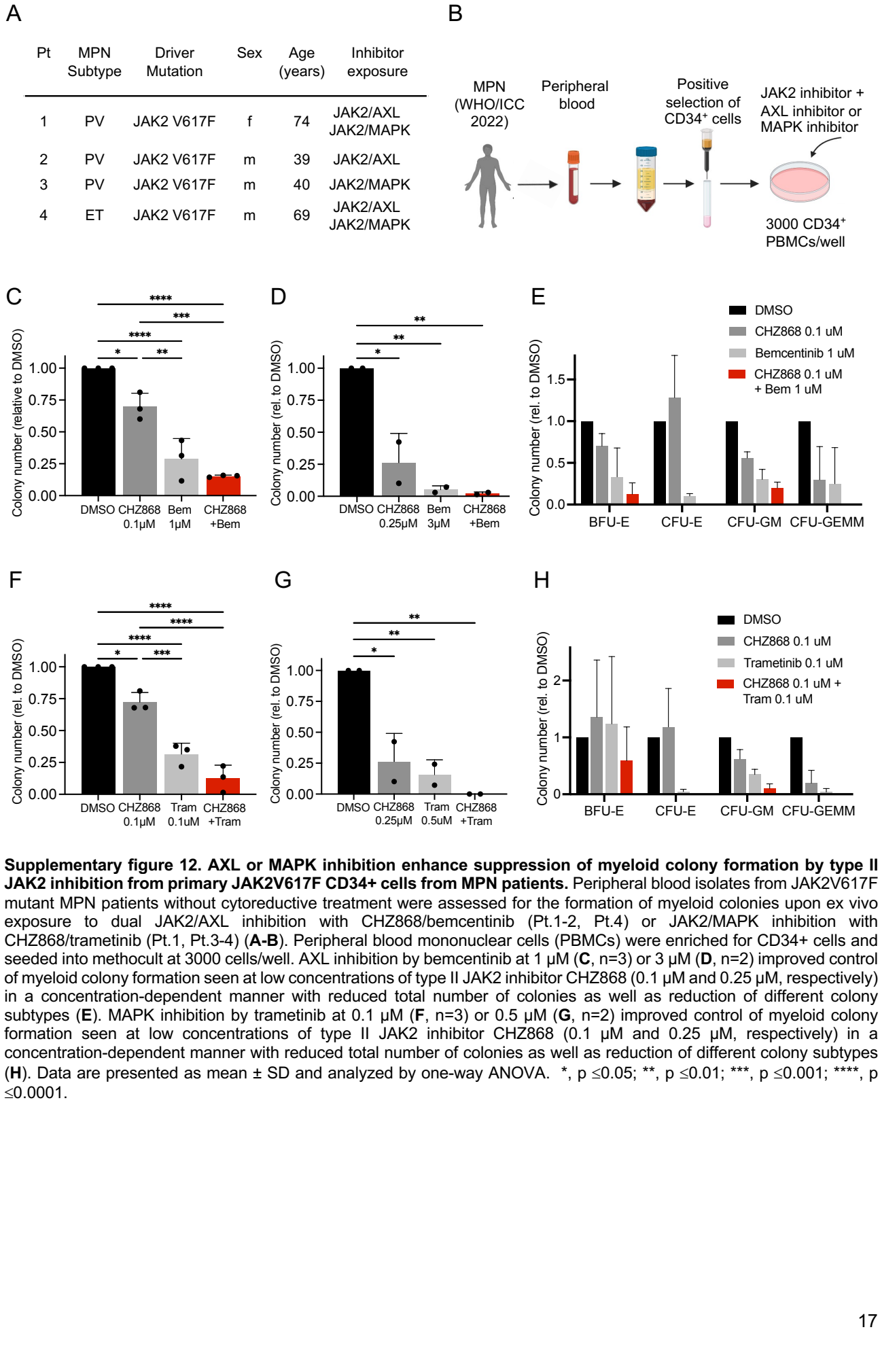

Supplementary figure 12. AXL or MAPK inhibition enhance suppression of myeloid colony formation by type II JAK2 inhibition from primary JAK2V617F CD34+ cells from MPN patients. Peripheral blood isolates from JAK2V617F mutant MPN patients without cytoreductive treatment were assessed for the formation of myeloid colonies upon ex vivo exposure to dual JAK2/AXL inhibition with CHZ868/bemcentinib (Pt.1-2, Pt.4) or JAK2/MAPK inhibition with CHZ868/trametinib (Pt.1, Pt.3-4) (**A-B**). Peripheral blood mononuclear cells (PBMCs) were enriched for CD34+ cells and seeded into methocult at 3000 cells/well. AXL inhibition by bemcentinib at 1 μM (**C**, n=3) or 3 μM (**D**, n=2) improved control of myeloid colony formation seen at low concentrations of type II JAK2 inhibitor CHZ868 (0.1 μM and 0.25 μM, respectively) in a concentration-dependent manner with reduced total number of colonies as well as reduction of different colony subtypes (**E**). MAPK inhibition by trametinib at 0.1 μM (**F**, n=3) or 0.5 μM (**G**, n=2) improved control of myeloid colony formation seen at low concentrations of type II JAK2 inhibitor CHZ868 (0.1 μM and 0.25 μM, respectively) in a concentration-dependent manner with reduced total number of colonies as well as reduction of different colony subtypes (**H**). Data are presented as mean ± SD and analyzed by one-way ANOVA. *, p ≤0.05; **, p ≤0.01; ***, p ≤0.001; ****, p ≤0.0001.